Fuel 307 (2022) 121796

Contents lists available at ScienceDirect

Fuel

journal homepage: www.elsevier.com/locate/fuel

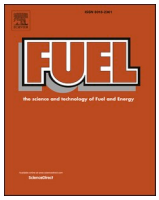

Full Length Article

The effect of coal viscosity-temperature characteristics on the dynamic response of slag discharge behavior in Shell gasifier

Kuo Lin [a,b], Zhongjie Shen [a,b], Qinfeng Liang [a,b], Zhenghua Dai [a,b], Jianliang Xu [a,b,*], Xiaolei Guo [a,b], Haifeng Liu [a,b]

[a] Shanghai Engineering Research Center of Coal Gasification, East China University of Science and Technology, P.O. Box 272, Shanghai 200237, PR China
[b] Institute of Clean Coal Technology, East China University of Science and Technology, P. O. Box 272, Shanghai 200237, PR China

ARTICLE INFO

Keywords:
Shell gasifier
Dynamics response
Gas-slag separation
Slag blocking
Operating temperature
Viscosity-temperature

ABSTRACT

How to efficiently and quickly detect the slag blocking behavior of entrained flow gasifiers was an urgent engineering problem. At present, the syngas composition of the gasifier was usually detected to judge whether slag plugging occurred, which had significant hysteresis. In this study, based on the slag dynamic flow model, the influences of operating conditions and slag viscosity-temperature characteristics on the slag discharge behavior of shell gasifiers were investigated. The results showed that the viscosity-temperature characteristics of slag had a great influence on the slag flow response process. The slag steady time and the corresponding steady thickness increased gradually with the transformation of slag type from glassy slag to crystalline slag. When the critical viscosity increased from 9.66 Pa·s to 43.5 Pa·s, the total slag thickness of glassy slag B and crystalline slag D increased by 6.4 and 10.5 cm, respectively. Besides, the slag steady time increased exponentially with the decrease of operating temperature. When the operating temperature dropped by 90 K, the steady-state time of the crystalline slag D reached 210 h.

1. Introduction

As one of the primary energy sources, coal played an important role in the chemical, metallurgy and power industries [1]. Especially considering that the duration of oil reserves would be much shorter than that of coal reserves in the world, coal had an increasingly important status [2,3]. In order to make efficient use of coal resources and reduce carbon emissions, a large number of efforts had been implemented to develop clean coal technology.

The entrained-flow coal gasification was an essential technology to convert the inorganic matter of coal into H_2 and CO in a clean and efficient way [4,5]. Due to its wide fuel adaptability, it was the main trend of the large-scale industrial gasification plant [6]. In order to ensure high gasification efficiency, the operating conditions of high temperature and high pressure were adopted in the entrained-flow gasifier [7]. Under this circumstance, the residual minerals and carbon after gasification deposited on the refractory wall where they formed the liquid slag layer and then flowed into the water-cooled pool through the slag tapping hole [8,9]. At present, many types of entrained-flow gasifiers had been commercially applied, including Shell gasifier, SE gasifier, OMB gasifier, Texaco gasifier and so on [10]. Shell gasifier, as one of the typical coal gasification technologies, had been introduced by China for a long time and was still adopted by many gasification projects. Industrial operation records [11] showed that slag plugging was the most common operation problem faced by Shell gasifier as shown in Fig. 1. There were often large-scale slag blocks directly plugging the outlet of the water-cooled pool, or slag continued to accumulate or even enter the gasification chamber, which were unfavorable to the long-term stable operation.

Due to the difficulty of in-situ measurement within the gasifier, the composition of the downstream syngas was usually monitored in the commercial gasifier, which was regarded as the indicator of slag thickness and gas temperature [12]. However, there was a certain delay between these parameters. In fact, numerical modeling of the slag layer was an efficient and convenient way to predict the slag flow process in the commercial gasifier [13,14]. The analytical model was obtained by the analysis of the mass, momentum, and energy conversation equations. It was assumed that the slag temperature reached the temperature of critical viscosity as the boundary between liquid slag and solid slag [14–16]. The most classical model was built by Seggiani [17], which modeled the time-varying slag flow process in a Prenflo entrained-flow

* Corresponding author.
E-mail address: xujl@ecust.edu.cn (J. Xu).

https://doi.org/10.1016/j.fuel.2021.121796
Received 27 May 2021; Received in revised form 4 August 2021; Accepted 23 August 2021
Available online 10 September 2021

Nomenclature

A	unit area (m^2)
g	gravitational acceleration (m/s^2)
m_{ex}	slag mass outflow rate per unit (kg/s)
m_{in}	mass flow rate of depositing particle (kg/s)
Q	heat flux (W)
T_{cv}	temperature of critical viscosity of slag (K)
T_g	temperature of gas temperature in furnace (K)
T_s	slag interfcae temperature (K)
T_{ss}	slag surface temperature (K)
T_m	mean temperature of metal wall (K)
T_r	mean temperature of refractory layer (K)
T_w	surface temperature of refractory layer (K)
u_i	flow velocity of molten slag (m/s)

Greek letters

δ	Total slag thickness (m)
δ_s	solid slag thickness (m)
δ_l	liquid slag thickness (m)
ρ	slag density (kg/m^3)
τ	shear force
μ_s	slag viscosity (Pa·s)
λ	thermal conductivity of slag (W/m·K)

gasifier. The energy equation of slag could be derived by assuming that the temperature distribution of slag was linear. Troiano et al. [18] studied the interaction of micromechanics of char/ash particles with a surface. Considering the effect of the particles' impact velocity and the residual carbon content, the particle deposition models were closured. Based on the adoption and modification of Seggiani's model, Bi et al. [19] studied the slag flow behavior in the refractory brick lining and membrane wall lining gasifier. Considering that the change of slag thermal conductivity, the temperature profile across the slag layer was cubic rather than linear. Montagnaro et al. [20] studied the fate of coal particles in the slagging regime. After detailedly analyzed the effects of turbulence-promoted particle migration toward the wall, a 1D model of the particle deposition process was proposed. These models were proved to be reliable by comparing with the experimental data.

For most types of entrained flow gasifiers, slag flowed downward along the wall driven by gravity and gas-phase shear force, and the direction of slag flow was the same as that of gas flow. However, due to the special structure of the water-cooled pool of Shell gasifier, the gas swirled downward and forms an updraft flow at the center, which left the cool pool area again, as shown in Fig. 2. And the influence of gas-flow on the slag flow process was more complex. For example, the negative pressure in the local area could lead to more slag entrained with the gaseous flow [21]. Besides, the determination of the slag response characteristic time was important when the abnormal conditions occurred in the gasifier. When the operating conditions in the gasifier changed, if the response time of the slag layer could be determined based on different slag types, it was helpful to guide the industrial gasifier to make more reasonable countermeasures. Therefore, it was necessary to study the blockage behavior based on the slag types to improve the coal adaptability of the Shell gasifier.

The particle deposition process was much rapid and the deposition process was often completed in tens of seconds [22,23]. However, the

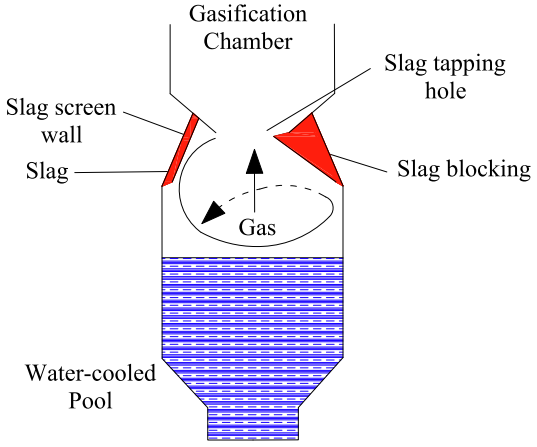

Fig. 2. Schematic diagram of discharging slag system of Shell gasifier.

Fig. 1. The blocking of slag discharge system of Shell gasifier.

slag response process often took several hours or even longer. Considering the difference of time scale between particle deposition process and slag flow process, the coupling of furnace flow field numerical model and the dynamic response model of slag flow greatly improved the accuracy and efficiency of the calculation. In this study, the combination of Seggiani's model [17] and Xu's simulation method [24,25] was presented. According to our previous work [26], the viscosity-temperature characteristics of different types of slags were proposed. Based on the dynamics model of slag flow and heat transfer, the effects of slag types, slag viscosity-temperature characteristics and operating temperature on the slag flow response process in Shell gasifier were studied. And the characteristic response time of the slag layer was analyzed.

2. Methodology

2.1. Model description

2.1.1. The slag flow and heat transfer model

The slag discharging system of the Shell gasifier was selected as the object in this study, whose structure was shown in Fig. 2. The lower temperature of the bottom area of the slag tapping hole made slag plugging more likely to occur compared to other areas. Therefore, the slag plugging characteristics of the bottom area of the slag tapping hole was studied in this work. The following assumptions were introduced here to describe the slag flow at the slag tapping hole region.

(1) Due to the magnitude of heat transfer, only the radial heat transfer behavior was considered.
(2) The change of slag temperature caused by slag evaporation was ignored.
(3) The interface between the solid and liquid slag layers was tracked at T_s ($\mu = 100$ Pa·s).
(4) The exponential function was used to describe slag viscosity.
(5) Except for the slag viscosity and thermal conductivity, the other physical parameters including the slag density and specific heat were constants.

The temperature range of the inner wall surface of the membrane wall gasifier was approximately 1400 ~ 1600 K along the axial direction, but its temperature range along the radial direction was approximately 1500 ~ 500 K. Compared with the radial temperature gradient, the axial temperature gradient of the gasifier was significantly small [24]. Therefore, Assumption 1 believed that the heat transfer only occurred in the radial direction in the two-dimensional heat transfer process. The slag tapping hole was located at the lower part of the gasifier, where the resources of slag-flow mainly came from the inflow of the top area. The low particle deposition rate determined the influence of inactive slag evaporation on the slag heat transfer process was relatively slight. To simplify the modeling process, the slag evaporation process was ignored in Assumption 2.

Wang et al. [27] studied the slag deposition and growth at the slag tap hole region of the Shell gasifier. In their works, the method that slag temperature reached the temperature of critical viscosity was the basis for distinguishing liquid–solid slag was followed. However, the slag viscosity actually varied greatly below the temperature of critical viscosity for different types of slag. For the crystalline slag, the decrease of temperature led to the sharp increase of the viscosity of the slag near the critical temperature, so that the slag hardly flowed [28–30]. On the contrary, in a wide temperature range below the temperature of critical viscosity, the glassy slag still had a high fluidity with the decrease of temperature [31]. Therefore, this method was not applicable to all slag types, and it often causes relatively large errors. To improve the accuracy, the concept of interface viscosity was adopted in this study [26]. The interface viscosity was a special value of the slag viscosity (Assumption 3), whose physical meaning was the highest viscosity at which the slag could flow [26]. According to the relevant literature [26,32–34], the interface viscosity was 100 Pa·s. Therefore, the thicknesses of the solid and liquid slag layers were separately determined by post-processing the temperature profile as follows:

$$\delta_s = \delta \frac{e^{bT_s} - e^{bT_w}}{e^{bT_{ss}} - e^{bT_w}} \tag{1}$$

It was found that the exponential function could well describe the viscosity-temperature curve in our previous work [26]. Compared with the slag viscosity, other physical properties of slag including specific heat and density had relatively little effect on the slag thickness. Therefore, Assumptions 4 and 5 were also reasonable. Based on the method proposed by Seggiani [17], the dynamics model of slag flow and heat transfer model was built. The wall was divided into 12 control units along the axial direction. Combined with the energy conservation equations for the SiC and membrane wall (Eqs. (4) and (5)), the slag momentum, mass and energy conservation equations (Eqs. (1)–(3)) in every unit were solved. The detailed modeling method could be found in Ref [17].

$$\frac{d}{dx}\left(\mu_s \frac{du_i}{dx}\right) = -\rho g \cos\beta, \begin{cases} x = 0, \mu_s \dfrac{du_i}{dx} = \tau \\ x = \delta_l, u_i = 0 \end{cases} \tag{2}$$

$$\rho A \frac{d\delta}{dt} = m_{in} + m_{ex,i-1} - m_{ex,i} \tag{3}$$

$$\rho_s c_s A_i \frac{d(\delta_l T_s)}{dt} = Q_{in} + Q_{out} + \frac{\mathrm{m}_{in} c T_{g,i} + \Delta q_{ex,i}}{A_i} \tag{4}$$

$$\rho_r \delta_r c_r A_r \frac{d(T_r)}{dt} = Q_{out} - Q_m \tag{5}$$

$$\rho_m \delta_m c_m A_m \frac{d(T_m)}{dt} = Q_m - Q_{mo} \tag{6}$$

2.1.2. Two-dimensional gasifier model

In this work, a two-dimensional symmetrical model was established to simulate the flow field within the gasifier. Xu's method [24,25] was adopted to simulate the flow field in the gasifier. Reynolds Averaged Navier Stokes equations which were used to model the gas-phase turbulent flow, as well as the mass and energy conservation equations, were solved. The realizable k–ε model with QUICK discretization scheme was used to predict the swirling flow. The random trajectory model was adopted to track each particle in Lagrangian coordinates. The eddy dissipative concept model, a random pore model, moisture vaporization model [35] and standard wall function were used to simulate homogeneous reaction, heterogeneous reaction, water evaporation and the gas flow on the wall. The gas shear force model was adopted according to our previous work [36]. The adhesion model proposed by Chen et al. [37] was used as the simulation model for particle deposition. The P1 model simulated radiation heat transfer. Further information was provided in Xu et al [24,25].

2.2. Algorithm

A Shell pulverized coal gasifier, whose scale was consistent with industrial plants, was selected as a research object in this study. Based on Fluent, the numerical simulation of the gasification core zone was built. Considering the axisymmetric structure of the water-cooled pool, the simulation region was set to a quarter of the gasifier in order to reduce the computational load. The two-order upwind scheme was used to discretize the governing equations. The simulation was operated with the pressure-based solver and was solved by SIMPLE algorithm. The output results of the numerical simulation including the heat flux and particle deposition rate were used as the input parameters of the dynamic model of slag heat and transfer. Combined with the gas shear

force model, the slag heat and heat transfer models were solved by the user-defined code in Matlab software. The momentum, energy and mass conservation were nonlinear differential equations, which were solved by the Runge-Kutta method. Besides, the trapezoidal integration method was used to obtain the slag mass flow rate. In the iterative calculation process, the time scale of each step was 1 s. When the relative error of all physical parameters was less than 0.00001 in every iterative time step ($\frac{P(t+1)-P(t)}{P(t)} < 0.00001$), the system was considered to be stable. The coupling process of different models is shown in Fig. 3.

2.3. Boundary conditions and material parameters

The operating pressure of the gasifier was 4.0 MPa, and the flow rates of coal and oxidant in each nozzle were 5.68 kg/s. and 5.375 kg/s. The slag layer was composed of liquid and solid slags due to the high heat flux. The liquid slag was distributed onto the surface of the slag layer and flowed from top to bottom under the action of gravity and gas shear force. The purpose of this work was to study the dynamic response of slag discharge behavior based on the coal viscosity-temperature characteristics. Compared with the slag viscosity, other parameters had a relatively little effect on slag thickness. Therefore, the other parameters of different slags including slag thermal conductivity, specific heat and density were considered to be the same. According to the relevant literature [38], the slag thermal conductivity could be expressed as an exponential function. The specific heat and density of the slag were 1670 J/(kg·K) and 2535 kg/m^3, respectively [17]. The coal proximate analysis and ultimate analysis are shown in Table 1.

The temperature-viscosity property (Newton fluid region) of the blending slag was measured using a high temperature rotational viscometer (Theta Industries, Port Wash, N Y). Besides, the slag viscosity-temperature characteristics below the temperature of critical viscosity were constructed according to our previous work [26] and could be expressed as follows:

$$\mu = \begin{cases} \mu_{cv} e^{-b(T-T_{cv})}, T < T_{cv} \\ \mu_{cv} e^{-a(T-T_{cv})}, T > T_{cv} \end{cases} \quad (7)$$

The viscosity-temperature characteristic parameters of different slag types, different critical viscosities and different temperatures of critical viscosity are shown in Tables 2-4. Although the viscosity curves of slag A ~ D were virtually constructed, they were approximately the same as that of several representative slags. For example, slag A was an ideal glass slag. Slag B, slag C and slag D were glassy slag, plastic slag and crystalline slag D, respectively. The detailed constructed process and the curves of viscosity temperature could be found in the supplemental material section.

3. Results and discussion

3.1. Temperature response behavior with transient operating temperature

At present, the operating temperature was usually approximately determined by the temperature of critical viscosity or fluid temperature in industrial operation. Therefore, in order to facilitate industrial reference, ΔT was defined as the difference between the operating temperature and the temperature of critical viscosity in this study. Considering that some abnormal operating conditions often occurred, a wide range of operating temperatures was selected. For the studied gasifier, the discharge system reached stability when $\Delta T = 100K$. At this time, the slag discharge temperature was changed to $\Delta T = 10K$ instantaneously. The mean temperature distributions of slag and SiC with different slag types were shown in Figs. 4 and 5. With the decrease of operation temperature, the mean temperature of different slags would decrease. With the slag types transformation from glass slag to crystalline slag, the time for slag mean temperature to reach stability became longer and the steady temperature amplitude slightly decreased. For glassy slag A and B, the slag mean temperatures were stable in approximately 4 h after the change of operating temperature. For plastic slag C and crystalline slag D, a longer steady time was needed. The changing trend of SiC mean temperature was in accordance with the slag mean temperature. However, compared with the temperature change amplitude of the slag layer, the change of slag type had a more significant impact on that of the SiC layer. With the decrease of operating temperature, the mean temperature of SiC fed with slag A, B, C and D decreased by 54, 79, 109 and 119 K, respectively.

3.2. Slag thickness response behavior with transient operating temperature

There were some important physical properties of slag, such as thermal conductivity, specific heat and viscosity, which had an important influence on the slag flow process. However, according to the previous research [39,40], the differences in specific heat and thermal conductivity between different slags were relatively slight. The main factor leading to the great difference of slag flow state among different slag types was the slag viscosity-temperature characteristics. At present, the critical viscosity (corresponding to the temperature of critical viscosity), the temperature of critical viscosity and the crystalline state of slag (lower than the temperature of critical viscosity) were generally used to characterize the slag viscosity [21]. In some previous studies [26,41,42], the slag viscosity was approximately described by a piecewise exponential function with different curvatures. The predicted results were approximately consistent with the experimental values, therefore this method was used in this study. When the temperature was lower than the temperature of critical viscosity, the curvature b of slag actually represented the type of slag. With the increase of b, the glassy

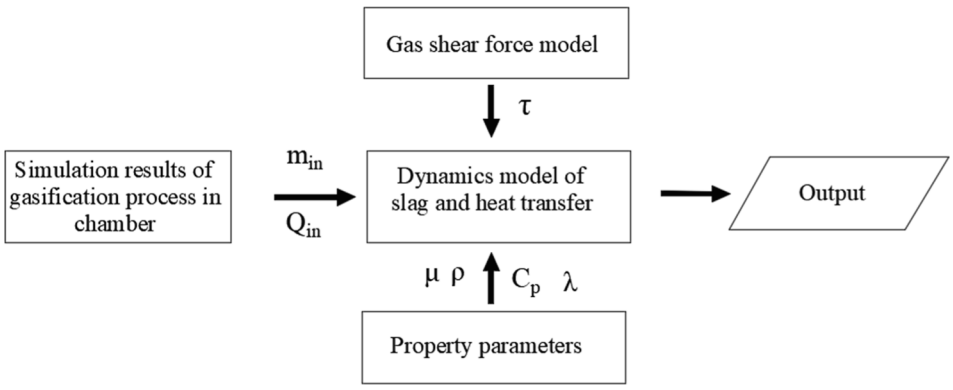

Fig. 3. The integration of different models.

Table 1
Coal proximate analysis and ultimate analysis.

Proximate analysis (%d)			HHV(d)	Ultimate analysis (%d)				
A	V	FC	MJ/kg	C	H	O	N	S
10.43	72.21	76.91	28.459	76.910	3.442	1.002	0.817	0.469

Table 2
The viscosity-temperature characteristic parameters of different types of slags.

Types	$T > T_{cv}$		$T < T_{cv}$	
Slag	T_{cv}	μ_{cv}	a	b
A	1623	29.6	0.012	0.012
B	1623	29.6	0.012	0.021
C	1623	29.6	0.012	0.078
D	1623	29.6	0.012	1.0

Table 3
The viscosity-temperature characteristic parameters of slags B and D with different critical viscosities.

Types	$T > T_{cv}$		$T < T_{cv}$	
Slag	T_{cv}	μ_{cv}	a	b
B_1	1623	9.66	0.012	0.021
B_2	1623	14.5	0.012	0.021
B_3	1623	29.6	0.012	0.021
B_4	1623	43.5	0.012	0.021
D_1	1623	9.66	0.012	1.0
D_2	1623	14.5	0.012	1.0
D_3	1623	29.6	0.012	1.0
D_4	1623	43.5	0.012	1.0

Table 4
The viscosity-temperature characteristic parameters of slag B with different temperatures of critical viscosity.

Types	$T > T_{cv}$		$T < T_{cv}$	
Slag	T_{cv}	μ_{cv}	a	b
B_1'	1423	29.6	0.012	0.021
B_2'	1523	29.6	0.012	0.021
B_3'	1623	29.6	0.012	0.021
B_4'	1723	29.6	0.012	0.021
B_5'	1823	29.6	0.012	0.021

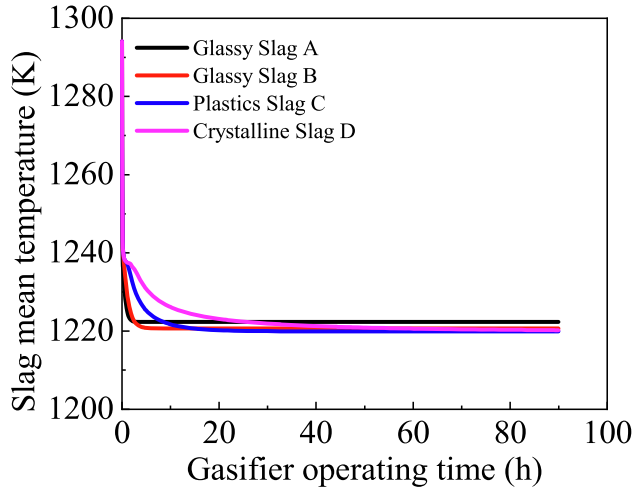

Fig. 4. Mean temperature distribution of slag layer with different slag types.

slag gradually transformed into crystalline slag. In this section, in order to study the flow state of different slags, the influence of viscosity-temperature characteristic parameter b, the temperature of critical viscosity and the critical viscosity on the response process of slag thickness was studied.

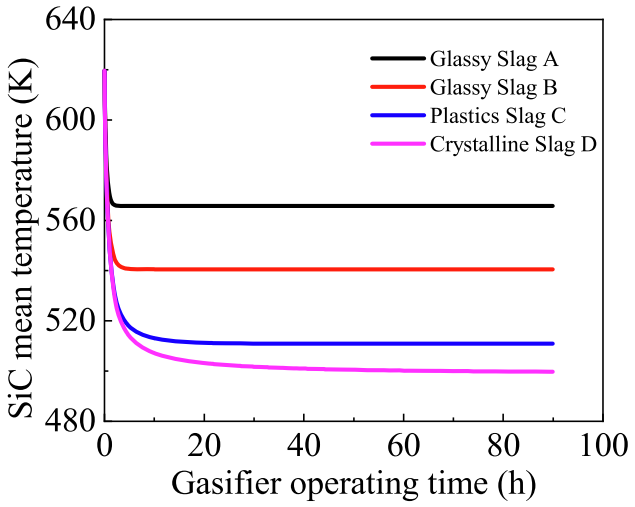

Fig. 5. Mean temperature distribution of SiC layer with different slag types.

3.2.1. The influence of slag types (b)

With the transient decrease of the operating temperature, the response process of the different slag thicknesses is shown in Fig. 6. The liquid slag thickness showed an obvious increase in the first 5 h, and then the changing trend slowed down and tend to be stable after more than 10 h. Compared with glassy slag A and B, the viscosity of plastic slag C and crystalline slag D increased more significantly with the decrease of temperature. Under the condition of the total amount of deposition remained unchanged, more liquid slag was transformed into solid slag. Therefore, the increased amplitude of plastic slag C and crystalline slag D was lower than that of glassy slag A and B, which could be supported by Fig. 6(b). With the decrease of operating temperature, the solid thickness of different slags increased, but the increased amplitudes were much different. The solid thicknesses of plastics slag C and crystalline slag D were up to 15.8 cm and 40.6 cm. And The solid thickness of glassy slag A and B were only 3.3 cm and 5.6 cm, respectively. Fig. 6(c) shows the response process of the total thicknesses of different slags with operating temperature changed. The response trend of total slag was consistent with that of solid slag due to that the thickness of solid slag was much higher than that of liquid slag.

3.2.2. The influence of critical viscosity

Fig. 7 shows the effect of critical viscosity on the response process of slag thickness. As the operating temperature decreased, the liquid slag thickness, solid slag thickness and total slag thickness all increased. And the increase of critical viscosity would further strengthen the increasing trend of slag thickness. However, the response amplitudes of different slags thickness to the change of critical viscosity were different. Compared with the liquid slag, the change of critical viscosity had more influence on the solid slag. For glassy slag B, when the critical viscosities were 9.66 Pa·s, 14.5 Pa·s, 29.0 Pa·s and 43.5 Pa·s, the liquid slag thicknesses were 0.37 cm, 0.38 cm, 0.40 cm and 0.48 cm, respectively. Correspondingly, the solid slag thicknesses were 2.6 cm, 3.3 cm, 5.3 cm and 9.0 cm, respectively. Besides, the thickness increase of crystalline slag D was higher than that of glassy slag B. When the critical viscosity

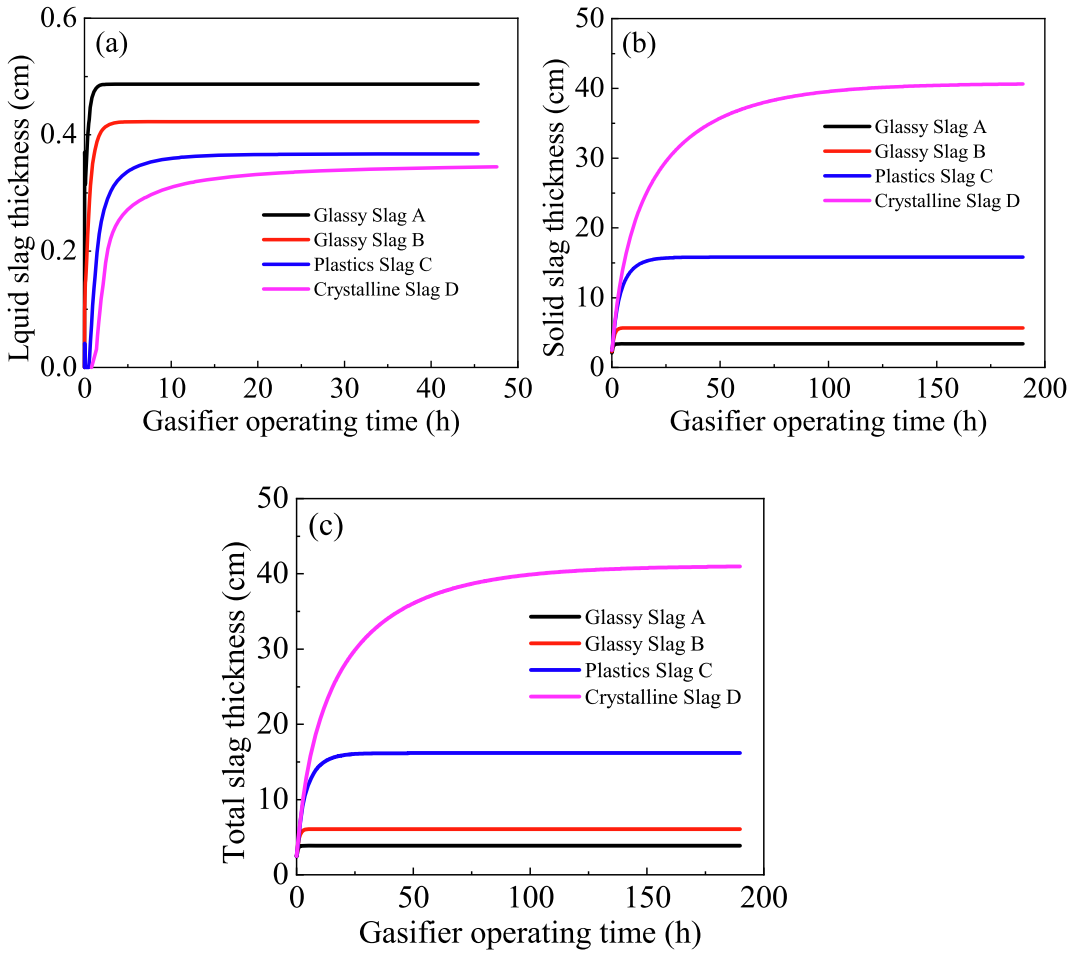

Fig. 6. Response process of the thicknesses of different types of slags with operating temperature changed (a: liquid slag; b: Solid slag; c: Total slag).

increased from 9.66 Pa·s to 43.5 Pa·s, the total slag thickness of crystalline slag D increased by 10.5 cm, while that of glassy slag B increased by 6.4 cm.

3.2.3. *The influence of the temperature of critical viscosity*

Under the condition of $\Delta T = 100K$, the discharge system reached stability. At this time the slag discharge temperature was instantaneously changed to $\Delta T = 10K$. Fig. 8 shows the effect of the temperature of critical viscosity on the response process of slag thickness. As mentioned above, the operating temperature ($\Delta T = T - T_{cv}$) was defined based on the temperature of critical viscosity in this study. Therefore, although ΔT was the same in this section, the absolute operating temperature would also increase with the increase of the temperature of critical viscosity. The results showed that with the increase of the temperature of critical viscosity, the thickness of the liquid slag layer decreased. On the contrary, the thickness of solid slag and total slag increased. Compared with the critical viscosity, the change of the temperature of critical viscosity had little effect on the thickness of the slag layer. This was consistent with our previous work [26] on the steady-state slag flow process.

3.3. *The characteristic response time of slag layer*

In the slag discharge system of the shell gasifier, the selection of temperature was critically important to be able to smoothly discharge slag. When the lower operating temperature was adopted, the slag tapping hole was easily blocked due to the increase of slag viscosity. If the high operating temperature was adopted, the slag blocking in the slag tapping hole could be avoided. However, the slag continued to flow downward and fell into the water-cooled pool after it flowed through the hole. And the formed liquid film would be stretched to become liquid filaments under the influence of the swirling flow. The liquid film and liquid filaments entrained by the gas flow adhered to the slag screen wall again, resulting in slag blocking. Besides, the transmission lag of the detection index often led to the untimely detection of slag plugging, which easily led to safety accidents. Therefore, the characteristic time for slag layer reaching stability was studied when the gasifier operating conditions changed in this section.

3.3.1. *The influence of slag viscosity-temperature characteristics*

When the operating temperature changed from $\Delta T = 100$K to $\Delta T = 10$K, the distributions of the time for slag reaching stability and the corresponding thickness with different viscosity-temperature characteristic parameters b are shown in Fig. 9. When the characteristics parameter b was lower than 0.5, the slag steady time increased rapidly with the increase of parameter b. The characteristics parameter b actually determined the type of slag. With the increase of b, the slag type gradually changed from glassy slag to crystalline slag. Therefore, when the operating temperature changed, more steady-state time more needed with the increase of parameter b. However, if the characteristics parameters b reached 0.5, the continuous increase of b had no effect on the steady time. It demonstrated that when parameter b exceeded approximately 0.5, the slag type was crystalline slag. Different crystalline slags showed the same characteristic: the viscosity increased rapidly below the temperature of critical viscosity, and the liquid–solid transition temperatures ($T_{\mu=100\text{Pa·s}}$) were almost equal. It could be concluded that different crystalline slags had almost the same steady-state time. The distribution of slag steady thickness with parameter b was similar to

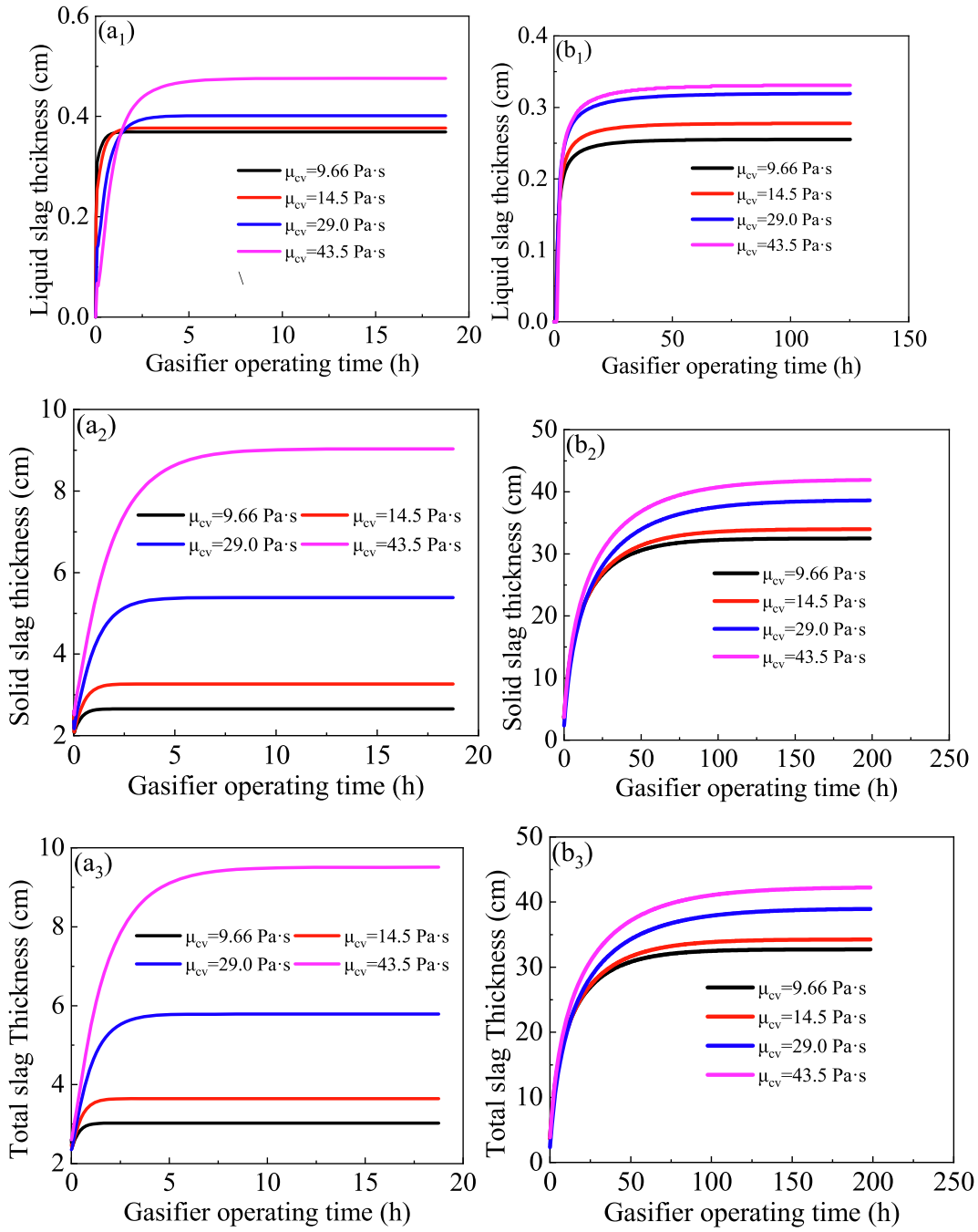

Fig. 7. The effect of critical viscosity on the response process of slag layer thickness (1: liquid slag, 2: solid slag, 3: total slag; a: glassy slag B, b: crystalline slag D).

that of the steady time. With the increase of *b*, the maximum thickness increased to 42 cm and remained constant. Referring to the operation records of commercial gasifiers, it was necessary to ensure that the effective cross-sectional area of the slag tapping hole was more than 85% in order to smooth and stable slag discharge. For the gasifier studied, the diameter of the slag tapping hole was 1.85 m. When the effective cross-sectional area of the slag tapping hole reached 85%, the thicknesses of both crystalline slag and glassy slag should be less than 7.1 cm. However, although the critical thicknesses of different slags were the same, higher operating temperatures were required in the actual operation process when the feeding coal was crystalline slag because the thickness of crystalline slag was more sensitive to the change of operating conditions. The characteristic value of slag steady-state time should be determined according to slag type. When the slag types were glassy slag, plastic slag and crystalline slag, the slag steady time was 1 ~ 60 h, 60 ~ 180 h and 180 ~ 210 h.

According to the viscosity-temperature curves of glassy slag B and crystalline slag D, viscosity-temperature curves with different critical viscosities were constructed (the viscosity-temperature characteristic parameters are listed in Table 2). Based on the viscosity-temperature curves with different critical viscosities, the effect of critical viscosity on the steady time and the steady slag thickness was studied, as shown in Fig. 10. The steady time and steady slag thickness both increased with the increase of critical viscosity. Besides, with the increase of critical viscosity, the slope of steady-state time and steady-state slag thickness also increased. It demonstrated that the high critical viscosity had more influence on the dynamic response process of slag thickness than the low critical viscosity.

According to the viscosity-temperature curve of glass slag B, viscosity-temperature curves with different temperatures of critical

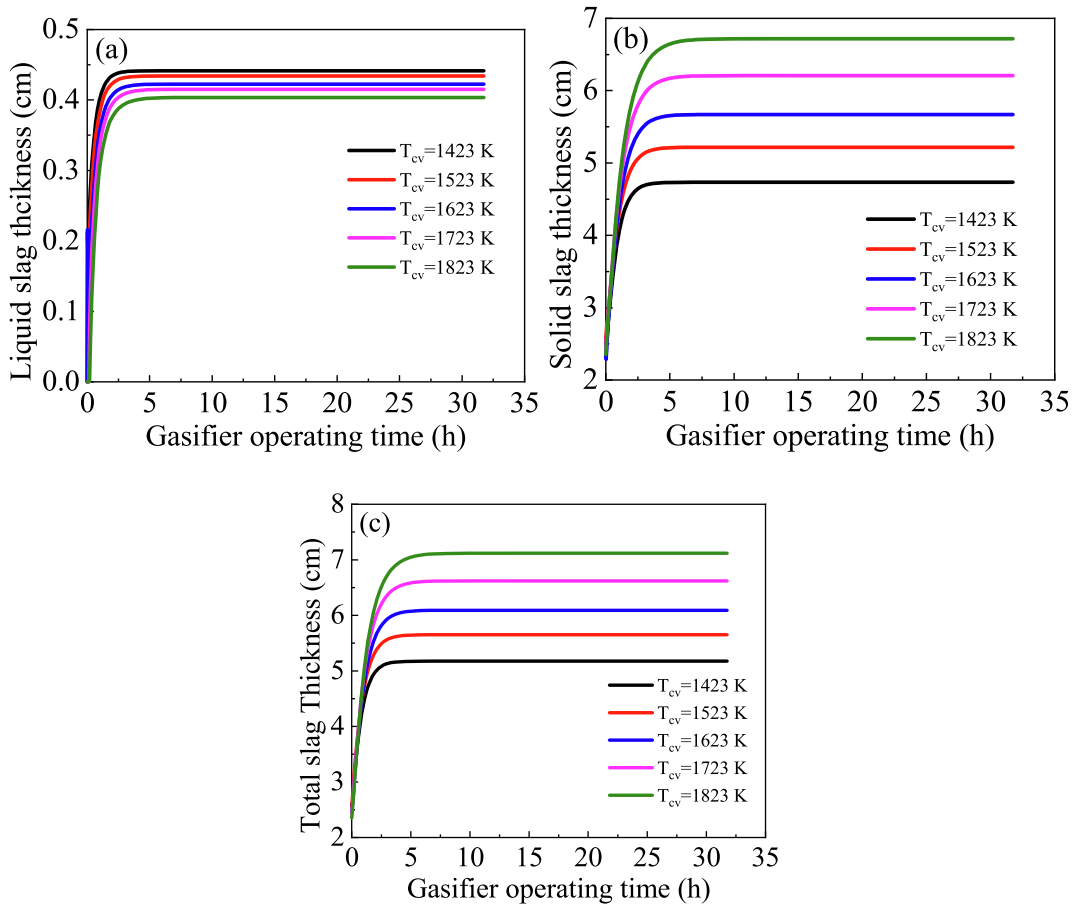

Fig. 8. The effect of the temperature of critical viscosity on the response process of slag B thickness (a: liquid slag; b: solid slag; c: total slag).

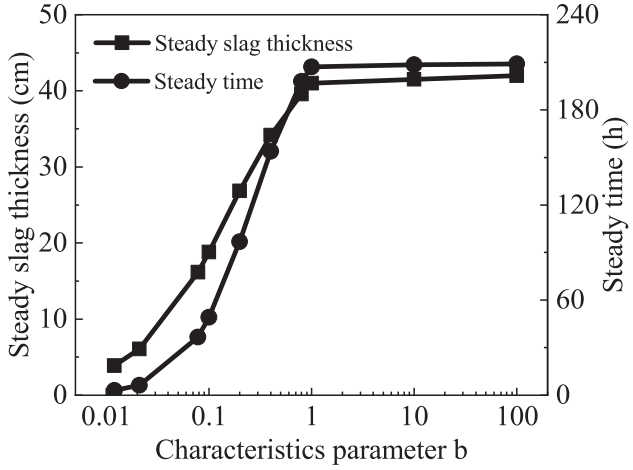

Fig. 9. The effect of the slag types on steady time and slag thickness.

viscosity were constructed (the viscosity-temperature characteristic parameters were listed in Table 3). Fig. 11 shows the effect of the temperature of critical viscosity on steady time and steady slag thickness. The results showed that the steady slag thickness and steady time increased linearly with the increase of the temperature of critical viscosity. As the temperature of critical viscosity increased from 1420 K to 1620 K, the steady time increased from 4.7 h to 8.0 h, and the steady slag thickness increased from 5.1 cm to 7.1 cm. Compared with critical viscosity, the change of the temperature of critical viscosity had little effect on the slag flow process.

3.3.2. *The influence of changing amplitude of operating temperature*

Slag flow was a complex physical and chemical process. On the one hand, the viscosity-temperature characteristics of slag could significantly affect the slag flow state. On the other hand, when the operating conditions changed, the slag discharge behavior would also show great differences. In Section 3.1–3.2, the slag discharge behavior was studied when the $\Delta T = 100$K. In this case, the slag could be discharged smoothly. In order to further study the slag discharge characteristics, the effects of transient decrease amplitudes ($\Delta T = 15, 30, 45 \cdots 90$ K) of operating temperature were investigated. Considering that when the feeding coal type was crystalline slag, the gasifier was easier to be blocked. Therefore, in this section, crystalline slag D was selected, as shown in Fig. 12. The steady-state time increased exponentially with the decrease of operating temperature. Especially at $\Delta T = 20$ K, any slight fluctuation of the operating temperature would cause a drastic change of the steady time. When the operating temperature continues to decrease to $\Delta T = 10$ K, the steady time was about 210 h. This meant that for the industrial-scale gasifier, there was a serious lag in the monitor the influence of the change of the operating temperature on the slag discharge behavior. When slag blocking occurred in the gasifier, the abnormal working conditions may begin to appear a few days ago.

3.4. *Discussion on smooth slag discharge of gasifier*

For the gas-slag cocurrent entrained-flow gasifier (e.g. OMB gasifier, Texaco gasifier and so on), once the slag tapping hole was blocked, the gas-flow would not flow out of the gasifier, leading to the increase of pressure inside the gasifier. Therefore, for the gas-slag cocurrent entrained-flow gasifier, whether slag plugging occurred could be determined by detecting the pressure drop inside furnace. However, for

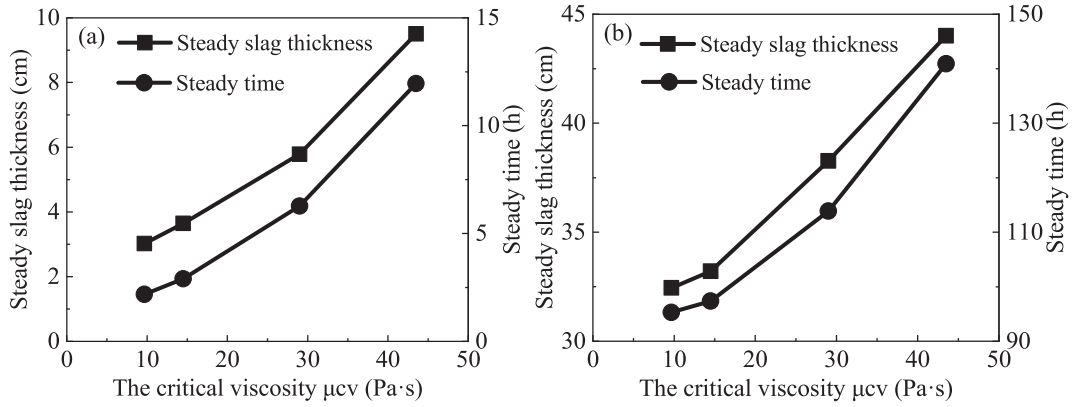

Fig. 10. The effect of the critical viscosity on steady time and slag thickness (a: glassy slag B;b: crystalline slag D).

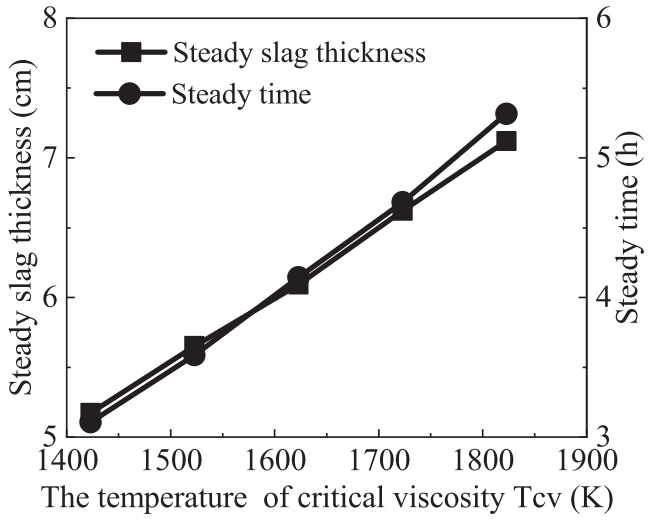

Fig. 11. The effect of the temperature of critical viscosity on steady time and slag thickness for slag B.

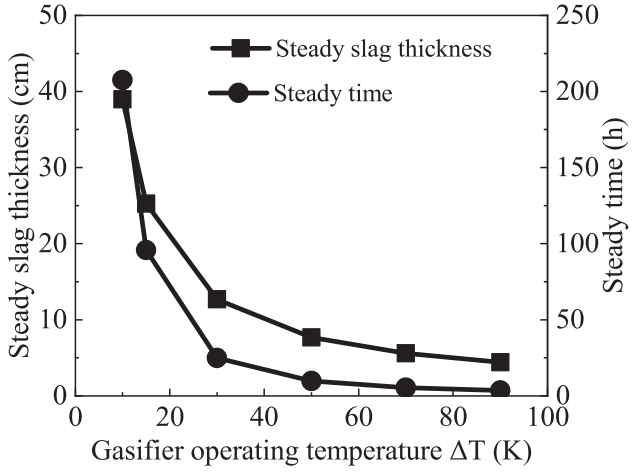

Fig. 12. The effect of the changing amplitude of operating temperature on steady time and steady slag thickness.

Shell Gasifier, the slag blockage would not prevent the gas-flow from flowing out the top of the gasifier due to the furnace structure of the gas-slag countercurrent. Therefore, it was useless to judge whether the gasifier was blocked by detecting the furnace pressure drop. In this circumstance, the method of judging whether slag plugging by detecting the metal wall temperature was much valuable (Fig. 5). According to a commercial scale Shell gasifier, the temperature of cooling water was about 493 K in this work. When the temperature of metal wall was lower than 520 K, it could be considered that the slag tapping hole was blocked.

In Section 3.3, the viscosity-temperature curves of crystalline slag, glassy slag and plastic slag were constructed. In addition, when the slag types were all glassy slag or crystalline slag, the viscosity-temperature curves with different critical viscosities and temperatures of critical viscosity were also constructed. Therefore, the slag viscosity-temperature characteristics constructed in this study basically covered most slag types. The slope of the viscosity curve (slag types, *b*), the temperature of critical viscosity and the critical viscosity were selected as influencing factors to study the slag discharge behavior in Section 3.3. The results showed that the selection of operating temperature must be based on slag type. Compared with crystalline slag, the acceptable operating temperature range of glassy slag was wider. For crystalline slag, a higher operating temperature was necessary to discharge slag smoothly. When the operating temperature changed, the slag steady time increased with the transformation of slag type from glassy slag to crystalline slag. In addition, the increase of critical viscosity and temperature of critical viscosity would also prolong the slag steady time.

For industrial gasifiers, how to avoid slag plugging was important. Besides, how to adjust the operating parameters to achieve smooth slag discharge again after slag blockage was also worthy. Fig. 12 shows the steady thickness and steady time of crystalline slag with different operating temperatures, which proposed specific reference values for alleviating the slag blockage of the industrial gasifier. According to above research on slag plugging process, it could be seen that the operating temperature was the key parameter to adjust the slag discharge for a given slag. When slag blockage occurred in the gasifier, it was necessary to increase the operating temperature (ΔT) to at least 50 K by adjusting the oxygen coal ratio, so that the slag block would melt and maintain the slag thickness at 5 cm. This process took approximately 9.7 h. It meant that the process of melting slag blocking was also a slow process.

4. Conclusion

Through the slag dynamic flow model, the slag discharge behavior of the Shell gasifier was studied. According to several typical virtually constructed viscosity-temperature curves, the effects of slag type, critical viscosity and temperature of critical viscosity on the slag discharge process were studied. The results showed that the operating temperature and the viscosity-temperature characteristics of slag could significantly affect the slag flow process. With the transformation of slag type from glassy slag to crystalline slag, the time for slag reaching steady state and

the corresponding thickness gradually increased. The slag steady time and slag steady thickness increased linearly with the increase of the temperature of critical viscosity. Compared with the temperature of critical viscosity, the critical viscosity had more significant influences on the slag steady time and the steady thickness. Besides, the steady-state time increased exponentially with the decrease of operating temperature.

CRediT authorship contribution statement

Kuo Lin: Investigation, Data curation, Writing - original draft. **Zhongjie Shen:** Visualization. **Qinfeng Liang:** Formal analysis. **Zhenghua Dai:** Methodology. **Jianliang Xu:** Methodology, Software, Supervision, Writing - review & editing. **Xiaolei Guo:** Conceptualization. **Haifeng Liu:** Conceptualization, Methodology, Supervision.

Declaration of Competing Interest

The authors declare that they have no known competing financial interests or personal relationships that could have appeared to influence the work reported in this paper.

Acknowledgement

This work was supported by the Shanghai Outstanding Technology Leader [Grant number 19XD1434800] and the National Natural Science Foundation of China [Grant number 21878082, 21776087].

Appendix A. Supplementary data

Supplementary data to this article can be found online at https://doi.org/10.1016/j.fuel.2021.121796.

References

[1] Shi J, Huang W, Han H, Xu C. Pollution control of wastewater from the coal chemical industry in China: Environmental management policy and technical standards. Renew Sust Energ Rev 2021;143:110883. https://doi.org/10.1016/j.rser.2021.110883.
[2] Dai B, Wu X, Zhang L. Establishing a novel and yet simple methodology based on the use of modified inclined plane (M-IP) for high-temperature slag viscosity measurement. Fuel 2018;233:299–308.
[3] Gai H, Feng Y, Lin K, Guo K, Xiao M, Song H, et al. Heat integration of phenols and ammonia recovery process for the treatment of coal gasification wastewater. Chem Eng J 2017;327:1093–101.
[4] Guo X, Li Y, Zhu Q, Hu X, Ma J, Guo Q. Reactivity of iron-based oxygen carriers with coal ash in pressurized chemical looping gasification. Fuel Process Technol 2021;219:106890. https://doi.org/10.1016/j.fuproc.2021.106890.
[5] Xue Z, Guo Q, Gong Y, Wang Y, Yu G. In-situ atomization and flame characteristics of coal water slurry in an impinging entrained-flow gasifier. Chem Eng Sci 2018;190:248–59.
[6] Ra HW, Mun T-Y, Hong SJ, Chun DH, Lee HT, Yoon SM, et al. Indirect coal liquefaction by integrated entrained flow gasification and Rectisol/Fischer–Tropsch processes for producing automobile diesel substitutes. Energy 2021;219:119597. https://doi.org/10.1016/j.energy.2020.119597.
[7] Ge Z, Kong L, Bai J, Chen X, He C, Li H, et al. Effect of CaO/Na_2O on slag viscosity behavior under entrained flow gasification conditions. Fuel Process Technol 2018;181:352–60.
[8] Wu G, Seebold S, Yazhenskikh E, Tanner J, Hack K, Müller M. Slag mobility in entrained flow gasifiers optimized using a new reliable viscosity model of iron oxide-containing multicomponent melts. Appl Energ 2019;236:837–49.
[9] Kondratiev A, Ilyushechkin A. Flow behaviour of crystallising coal ash slags: Shear viscosity, non-Newtonian flow and temperature of critical viscosity. Fuel 2018;224:783–800.
[10] Chen X, Kong L, Bai J, Dai X, Li H, Bai Z, et al. The key for sodium-rich coal utilization in entrained flow gasifier: The role of sodium on slag viscosity-temperature behavior at high temperatures. Appl Energ 2017;206:1241–9.
[11] Yan Y. A study on slag block in gasifier. Large Scale Nitrogenous Fertil Ind 2020;43:160–3.
[12] Kim M, Ye I, Ryu C. Numerical analysis on transient behaviors of slag layer in an entrained-flow coal gasifier. Fuel 2017;196:532–42.
[13] Lin K, Shen Z, Liang Q, Xu J, Liu H. Modelling study of characteristics of heat transfer and structural optimization of refractory layer in an entrained-flow gasifier. Appl Therm Eng 2020;168:114830. https://doi.org/10.1016/j.applthermaleng.2019.114830.
[14] Yang Z, Wang Z, Wu Y, Wang J, Lu J, Li Z, et al. Dynamic model for an oxygen-staged slagging entrained flow gasifier. Energy Fuels 2011;25(8):3646–56.
[15] Melchiori T, Boulet M, Lavoie J-M. Modeling of ash deposition on the wall of a high temperature slagging gasifier. Fuel 2017;197:100–10.
[16] Zhang B, Shen Z, Han D, Liang Q, Xu J, Liu H. Effects of the bubbles in slag on slag flow and heat transfer in the membrane wall entrained-flow gasifier. Appl Therma Eng 2017;112:1178–86.
[17] Seggiani M. Modelling and simulation of time varying slag flow in a Prenflo entrained-flow gasifier. Fuel 1998;77(14):1611–21.
[18] Troiano M, Solimene R, Montagnaro F, Salatino P. Char/ash deposition and near-wall segregation in slagging entrained-flow gasification of solid fuels: from experiments to closure equations. Fuel 2020;264:116864. https://doi.org/10.1016/j.fuel.2019.116864.
[19] Bi D, Guan Q, Xuan W, Zhang J. Combined slag flow model for entrained flow gasification. Fuel 2015;150:565–72.
[20] Montagnaro F, Salatino P. Analysis of char–slag interaction and near-wall particle segregation in entrained-flow gasification of coal. Combust Flame 2010;157(5):874–83.
[21] Cao Z, Li T, Zhang Q, Zhou H, Song C, You F. Systems modeling, simulation and analysis for robust operations and improved design of entrained-flow pulverized coal gasifiers. Energy 2018;148:941–64.
[22] Yang X, Ingham D, Ma L, Troiano M, Pourkashanian M. Prediction of particle sticking efficiency for fly ash deposition at high temperatures. Proc Combus Inst 2019;37(3):2995–3003.
[23] Han Z, Xu Z, Yu X, Sun A, Li Y. Numerical simulation of ash particles deposition in rectangular heat exchange channel. Int J Heat Mass Transf 2019;136:767–76.
[24] Xu J, Dai Z, Liu H, Guo L, Sun F. Modeling of multiphase reaction and slag flow in single-burner coal water slurry gasifier. Chem Eng Sci 2017;162:41–52.
[25] Xu J, Liang Q, Dai Z, Liu H. The influence of swirling flows on pulverized coal gasifiers using the comprehensive gasification model. Fuel Process Technol 2018;172:142–54.
[26] Lin K, Shen Z, Liang Q, Xu J, Guo X, Liu H. The study of slag discharge behavior of entrained-flow gasifier based on the viscosity-temperature characteristics of different types of coals. Fuel 2021;292:120314. https://doi.org/10.1016/j.fuel.2021.120314.
[27] Wang J, Liu H, Liang Q, Xu J. Experimental and numerical study on slag deposition and growth at the slag tap hole region of Shell gasifier. Fuel Process Technol 2013;106:704–11.
[28] Zhou J, Shen Z, Liang Q, Xu J, Liu H. A new prediction method for the viscosity of the molten coal slag. Part 2: The viscosity model of crystalline slag. Fuel 2018;220:233–9.
[29] Xuan W, Wang Q, Zhang J, Xia D. Influence of silica and alumina ($SiO_2 + Al_2O_3$) on crystallization characteristics of synthetic coal slags. Fuel 2017;189:39–45.
[30] Wang J, Guo Q, Wei J, Liu X, Wang X, Yu G. Understanding the influence of iron on fluidity and crystallization characteristics of synthetic coal slags. Fuel Process Technol 2020;209:106532. https://doi.org/10.1016/j.fuproc.2020.106532.
[31] Wang W, Dai S, Zhang T, Li Z, Xie Y. Effect of isothermal and cooling rate on crystallization and viscosity of silicomanganese waste slag. Ceram Int 2021;47(10):13622–7.
[32] Zhang B, Shen Z, Liang Q, Xu J, Liu H. Modeling the slag flow and heat transfer with the effect of fluid-solid slag layer interface viscosity in an entrained flow gasifier. Appl Therma Eng 2017;122:785–93.
[33] Ye I, Ryu C, Koo JH. Influence of critical viscosity and its temperature on the slag behavior on the wall of an entrained coal gasifier. Appl Therma Eng 2015;87:175–84.
[34] Yun Y, Yoo YD, Chung SW. Selection of IGCC candidate coals by pilot-scale gasifier operation. Fuel Process Technol 2007;88(2):107–16.
[35] Sun Z, Dai Z, Zhou Z, Guo Q, Yu G. Numerical Simulation of Industrial Opposed Multiburner Coal-Water Slurry Entrained Flow Gasifier. Ind Eng Chem Res 2012;51(6):2560–9.
[36] Lin K, Shen Z, Liang Q, Xu J, Guo X, Liu H. The effect of the shear force applied by gas-flow in furnace on slag flow characteristics and gasifier performance. Fuel Process Technol 2021;216:106794. https://doi.org/10.1016/j.fuproc.2021.106794.
[37] Chen L, Yong SZ, Ghoniem AF. Modeling the slag behavior in three dimensional CFD simulation of a vertically-oriented oxy-coal combustor. Fuel Process Technol 2013;112:106–17.
[38] Anderson DW, Viskanta R, Incropera FP. Effective thermal conductivity of coal ash deposits at moderate to high temperatures. J Eng Gas Turbines Power 1987;109:215–21.
[39] Tomeczek J, Palugniok H. Specific heat capacity and enthalpy of coal pyrolysis at elevated temperatures. Fuel 1996;75(9):1089–93.
[40] Rezaei H, Gupta RP, Bryant GW, Hart JT, Liu GS, Bailey CW, et al. Thermal conductivity of coal ash and slags and models used. Fuel 2000;79:1697–710.
[41] Ilyushechkin A, Kondratiev A, He C, Bai J, Chen X, Hla SS. Viscosity of spinel primary phase field slags from australian brown coals. Energy Fuels 2020;34(3):3041–56.
[42] Ilyushechkin A, Kondratiev A. Viscosity of slags with solids: The effect of solids morphology and concentration. J Rheol 2019;63(5):719–33.